Author/s:
Park, H;Crozier, KB

Title:
Elliptical silicon nanowire photodetectors for polarization-resolved imaging

Date:
2015-03-23

Citation:
Park, H. & Crozier, K. B. (2015). Elliptical silicon nanowire photodetectors for polarization-resolved imaging. Optics Express, 23 (6), pp.7209-7216. https://doi.org/10.1364/OE.23.007209.

Persistent Link:
https://hdl.handle.net/11343/116554

Elliptical silicon nanowire photodetectors for polarization-resolved imaging

Hyunsung Park[1] and Kenneth B. Crozier[1,2,3,*]

[1]*School of Engineering and Applied Sciences, Harvard University, 29 Oxford St., Cambridge, Massachusetts 02138, USA*

[2]*Department of Electrical and Electronic Engineering, University of Melbourne, VIC 3010, Australia*

[3]*School of Physics, University of Melbourne, VIC 3010, Australia*

[*]*kcrozier@unimelb.edu.au*

Abstract: Polarization-resolved imaging offers many advantages over conventional imaging because it provides additional information on materials and scenes. In this study, we present an image sensor pixel for polarization-resolved imaging based on an all-silicon nanowire device. As the structure has an intrinsically polarization-dependent response, it is not necessary to employ a polarizer. We fabricate pixels consisting of etched vertical silicon nanowires with elliptical cross-sections that incorporate vertical p-i-n junctions. Our photocurrent measurement reveals that the spectral responsivities are dependent on the polarization state of incident light. Polarization-resolved imaging is performed with fabricated devices. This approach is different from conventional approaches using polarization filters because absorbed light in the elliptical nanowire is converted to photocurrent while light absorbed by a polarization filter is discarded.

OCIS codes: (040.5160) Photodetectors; (110.5405) Polarimetric imaging; (230.5440) Polarization-selective devices; (220.4241) Nanostructure fabrication.

References and links

1. A. Sweeney, C. Jiggins, and S. Johnsen, "Insect communication: Polarized light as a butterfly mating signal," Nature **423**(6935), 31–32 (2003).
2. T. Labhart, "Polarization-opponent interneurons in the insect visual system," Nature **331**(6155), 435–437 (1988).
3. J. N. Lythgoe and C. C. Hemmings, "Polarized light and underwater vision," Nature **213**(5079), 893–894 (1967).
4. T. W. Cronin, N. Shashar, R. L. Caldwell, J. Marshall, A. G. Cheroske, and T.-H. Chiou, "Polarization vision and its role in biological signaling," Integr. Comp. Biol. **43**(4), 549–558 (2003).
5. V. Gruev, R. Perkins, and T. York, "CCD polarization imaging sensor with aluminum nanowire optical filters," Opt. Express **18**(18), 19087–19094 (2010).
6. S.-S. Lin, K. M. Yemelyanov, E. N. Pugh, Jr., and N. Engheta, "Separation and contrast enhancement of overlapping cast shadow components using polarization," Opt. Express **14**(16), 7099–7108 (2006).
7. J. O. Stenflo and H. Povel, "Astronomical polarimeter with 2-D detector arrays," Appl. Opt. **24**(22), 3893–3898 (1985).
8. W. Groner, J. W. Winkelman, A. G. Harris, C. Ince, G. J. Bouma, K. Messmer, and R. G. Nadeau, "Orthogonal polarization spectral imaging: A new method for study of the microcirculation," Nat. Med. **5**(10), 1209–1212 (1999).
9. E. Salomatina-Motts, V. A. Neel, and A. N. Yaroslavskaya, "Multimodal polarization system for imaging skin cancer," Opt. Spectrosc. **107**(6), 884–890 (2009).
10. Z. Nan, J. Xiaoyu, G. Qiang, H. Yonghong, and M. Hui, "Linear polarization difference imaging and its potential applications," Appl. Opt. **48**(35), 6734–6739 (2009).
11. J. S. Tyo, M. P. Rowe, E. N. Pugh, Jr., and N. Engheta, "Target detection in optically scattering media by polarization-difference imaging," Appl. Opt. **35**(11), 1855–1870 (1996).
12. M. P. Rowe, E. N. Pugh, Jr., J. S. Tyo, and N. Engheta, "Polarization-difference imaging: a biologically inspired technique for observation through scattering media," Opt. Lett. **20**(6), 608–610 (1995).
13. L. B. Wolff, T. A. Mancini, P. Pouliquen, and A. G. Andreou, "Liquid crystal polarization camera," IEEE Trans. Robot. Autom. **13**(2), 195–203 (1997).
14. A. G. Andreou and Z. K. Kalayjian, "Polarization imaging: principles and integrated polarimeters," IEEE Sens. J. **2**(6), 566–576 (2002).
15. Z. Xiaojin, F. Boussaid, A. Bermak, and V. G. Chigrinov, "Thin photo-patterned micropolarizer array for CMOS image sensors," IEEE Photon. Technol. Lett. **21**(12), 805–807 (2009).
16. V. Gruev, A. Ortu, N. Lazarus, J. Van der Spiegel, and N. Engheta, "Fabrication of a dual-tier thin film micropolarization array," Opt. Express **15**(8), 4994–5007 (2007).

17. M. Kulkarni and V. Gruev, "Integrated spectral-polarization imaging sensor with aluminum nanowire polarization filters," Opt. Express **20**(21), 22997–23012 (2012).
18. M. Law, J. Goldberger, and P. Yang, "Semiconductor nanowires and nanotubes," Annu. Rev. Mater. Res. **34**(1), 83–122 (2004).
19. J. Hu, T. W. Odom, and C. M. Lieber, "Chemistry and physics in one dimension: Synthesis and properties of nanowires and nanotubes," Acc. Chem. Res. **32**(5), 435–445 (1999).
20. Z. Fan, H. Razavi, J.-W. Do, A. Moriwaki, O. Ergen, Y.-L. Chueh, P. W. Leu, J. C. Ho, T. Takahashi, L. A. Reichertz, S. Neale, K. Yu, M. Wu, J. W. Ager, and A. Javey, "Three-dimensional nanopillar-array photovoltaics on low-cost and flexible substrates," Nat. Mater. **8**(8), 648–653 (2009).
21. J. C. Shin, K. H. Kim, K. J. Yu, H. Hu, L. Yin, C.-Z. Ning, J. A. Rogers, J.-M. Zuo, and X. Li, "$In_xGa_{1-x}As$ nanowires on silicon: One-dimensional heterogeneous epitaxy, bandgap engineering, and photovoltaics," Nano Lett. **11**(11), 4831–4838 (2011).
22. J. H. Ahn, H.-S. Kim, K. J. Lee, S. Jeon, S. J. Kang, Y. Sun, R. G. Nuzzo, and J. A. Rogers, "Heterogeneous three-dimensional electronics by use of printed semiconductor nanomaterials," Science **314**(5806), 1754–1757 (2006).
23. G. Zheng, W. Lu, S. Jin, and C. M. Lieber, "Synthesis and fabrication of high-performance n-type silicon nanowire transistors," Adv. Mater. **16**(21), 1890–1893 (2004).
24. L. Cao, P. Fan, E. S. Barnard, A. M. Brown, and M. L. Brongersma, "Tuning the color of silicon nanostructures," Nano Lett. **10**(7), 2649–2654 (2010).
25. L. Cao, J.-S. Park, P. Fan, B. Clemens, and M. L. Brongersma, "Resonant germanium nanoantenna photodetectors," Nano Lett. **10**(4), 1229–1233 (2010).
26. L. Cao, J. S. White, J.-S. Park, J. A. Schuller, B. M. Clemens, and M. L. Brongersma, "Engineering light absorption in semiconductor nanowire devices," Nat. Mater. **8**(8), 643–647 (2009).
27. S. K. Kim, R. W. Day, J. F. Cahoon, T. J. Kempa, K.-D. Song, H.-G. Park, and C. M. Lieber, "Tuning light absorption in core/shell silicon nanowire photovoltaic devices through morphological design," Nano Lett. **12**(9), 4971–4976 (2012).
28. K. Seo, M. Wober, P. Steinvurzel, E. Schonbrun, Y. Dan, T. Ellenbogen, and K. B. Crozier, "Multicolored vertical silicon nanowires," Nano Lett. **11**(4), 1851–1856 (2011).
29. H. Park and K. B. Crozier, "Multispectral imaging with vertical silicon nanowires," Sci Rep **3**, 2460 (2013).
30. H. Park, K. Seo, and K. B. Crozier, "Adding colors to polydimethylsiloxane by embedding vertical silicon nanowires," Appl. Phys. Lett. **101**(19), 193107 (2012).
31. H. Park, Y. Dan, K. Seo, Y. J. Yu, P. K. Duane, M. Wober, and K. B. Crozier, "Filter-free image sensor pixels comprising silicon nanowires with selective color absorption," Nano Lett. **14**(4), 1804–1809 (2014).
32. E. Schonbrun, K. Seo, and K. B. Crozier, "Reconfigurable imaging systems using elliptical nanowires," Nano Lett. **11**(10), 4299–4303 (2011).
33. D. Misra and E. L. Heasell, "Electrical damage to silicon devices due to reactive ion etching," Semicond. Sci. Technol. **5**(3), 229–236 (1990).
34. B. Wang and P. W. Leu, "Tunable and selective resonant absorption in vertical nanowires," Opt. Lett. **37**(18), 3756–3758 (2012).
35. B. C. P. Sturmberg, K. B. Dossou, L. C. Botten, A. A. Asatryan, C. G. Poulton, C. M. de Sterke, and R. C. McPhedran, "Modal analysis of enhanced absorption in silicon nanowire arrays," Opt. Express **19**(S5 Suppl 5), A1067–A1081 (2011).
36. T. York and V. Gruev, "Characterization of a visible spectrum division-of-focal-plane polarimeter," Appl. Opt. **51**(22), 5392–5400 (2012).

1. Introduction

Although the human eye can perceive the color of visible light, it is not sensitive to its polarization. By contrast, in other parts of the animal kingdom, eyes have evolved with polarization sensitivity [1–4]. Polarization provides important additional information on materials and scenes because it is affected by material characteristics, surface curvature, the angle of incident light, as well as other factors. For example, dark objects with small intensity variation can be clearly distinguished by degree-of-linear polarization [5,6], because it depends on surface curvature via the Fresnel reflection coefficients. These considerations have motivated the development of polarization-resolved imaging techniques for applications ranging from biological studies to remote sensing [7–11].

One simple way to capture a polarization-resolved image involves mounting a polarizer in front of a camera, mechanically rotating it to different orientations, and taking an image at each. In many cases, one would prefer to avoid mechanical rotation due to speed considerations. This has motivated the use of electrically-controlled liquid crystal polarization filters [12,13]. The bulk and speed limitations of this approach however will be problematic for many applications (e.g. imaging fast moving objects), despite being an improvement over the mechanical rotation of a polarization filter. The integration of micro-polarization filters

directly onto the image sensor is one solution to these limitations [5,14–17]. This approach is analogous to the use of Bayer color filters in image sensors, and enables the realization of compact systems that can perform polarization-resolved imaging at the frame rate of the image sensor, i.e. there is no temporal overhead associated with filter rotation, etc. These devices have limited efficiencies, however, as they function by absorbing or reflecting the undesirable polarized light. The light being absorbed in the polarization filter cannot be captured.

Semiconductor nanowires have been widely studied because of their unique electrical and optical characteristics [18–23]. Recently, it was demonstrated that horizontal semiconductor nanowires exhibit absorption spectra that can be engineered by appropriate choice of geometry [24–27]. We also demonstrated that vertical silicon nanowires shows vivid colors, as a result of wavelength-dependent spatial distribution of the waveguide mode [28]. Passive color filters for multi-spectral imaging [29,30] and filter-free image sensor pixels for color imaging [31] have been demonstrated using these characteristics. These nanowires are produced by lithography and dry etching [28–31]. A key benefit of this method is that the nanowire's cross-section, i.e. its shape and size, can be chosen at-will, being defined by lithography. Making use of this benefit, we demonstrated a polarization reconfigurable lens that comprised amorphous silicon nanowires with elliptical cross-sections [32].

Here, we demonstrate vertical silicon nanowire photodetectors with elliptical cross-sections. The elliptical nanowires have polarization dependent absorption, with the absorbed photons being converted to photocurrent and collected by integrated p-i-n junctions. Our measurements shows that the responsivities of fabricated devices have a polarization dependence and polarization-resolved imaging is performed. In our approach, no additional polarization filters, such as those based on metal wire grids and dichroic materials, are needed. Importantly, our method for polarization imaging is different from polarization filter based method. This is because the absorbed light in our method is not discarded but converted to photocurrent. As we discuss later, this fundamental difference between this and previous approaches could be employed in future devices to achieve higher efficiency.

2. Experimental results

Figure 1(a) shows the concept of our device. The elliptical nanowires have absorption spectra that depend on the polarization state of the illuminating light. We have previously shown [28,31] that vertical silicon nanowires with circular cross-sections exhibit absorption spectra containing peaks. The wavelength of each peak is highly dependent on the nanowire's radius, being determined by interplay between the coupling coefficient and confinement factor of a mode supported by the nanowire. Due to symmetry, the absorption spectra of circular nanowires are polarization-independent. By contrast, for elliptical nanowires, the absorption spectra differ depending on whether the light is polarized along the long or short axes. We use this phenomenon for polarization-resolved imaging.

We fabricated a device using epitaxial silicon wafers consisting of an n + type substrate with an n- type epitaxial layers (~1.5 μm thick, R > 100 Ω•cm) shown in Fig. 1(b). The top of the n- epitaxial layer is doped to p + using spin-on dopant (Poly Boron Film (PBF) 2.0A, Filmtronics) in a tube furnace (Lindberg Blue/M, Thermo Electron Corporation). The resultant thermal oxide produced in this process is completely removed using 5:1 buffered hydrofluoric acid. We spin coat polymethylmethacrylate (PMMA) to perform e-beam lithography to make arrays of ellipse patterns. We fabricate an aluminum (Al, 40 nm) etch mask using metal evaporation followed by the lift-off process. We dry etch the wafer to form nanowires with a height of 2.7 μm using inductively coupled plasma reactive ion etching (MPX/LPX RIE, Surface Technology Systems) with 62 / 160 sccm of SF_6 / C_4F_8 gases. The aluminum mask is then removed by a wet etching process (Type-A, Transene). PMMA (PMMA495-A8, Microchem) is spin-coated onto the nanowire sample. We then dry etch the top of the PMMA layer in an oxygen plasma (SCE106, Anatech LTD) until the tops of the nanowires are exposed. Indium tin oxide (ITO) with a thickness of 60 nm is then sputtered for a transparent top contact. The ITO layer is scribed to electrically separate the nanowire arrays

from one another. The device is then attached on a printed circuit board (PCB) and electrical connections are made to it using gold wires and silver conductive epoxy. The substrate of wafer is used as the bottom contact.

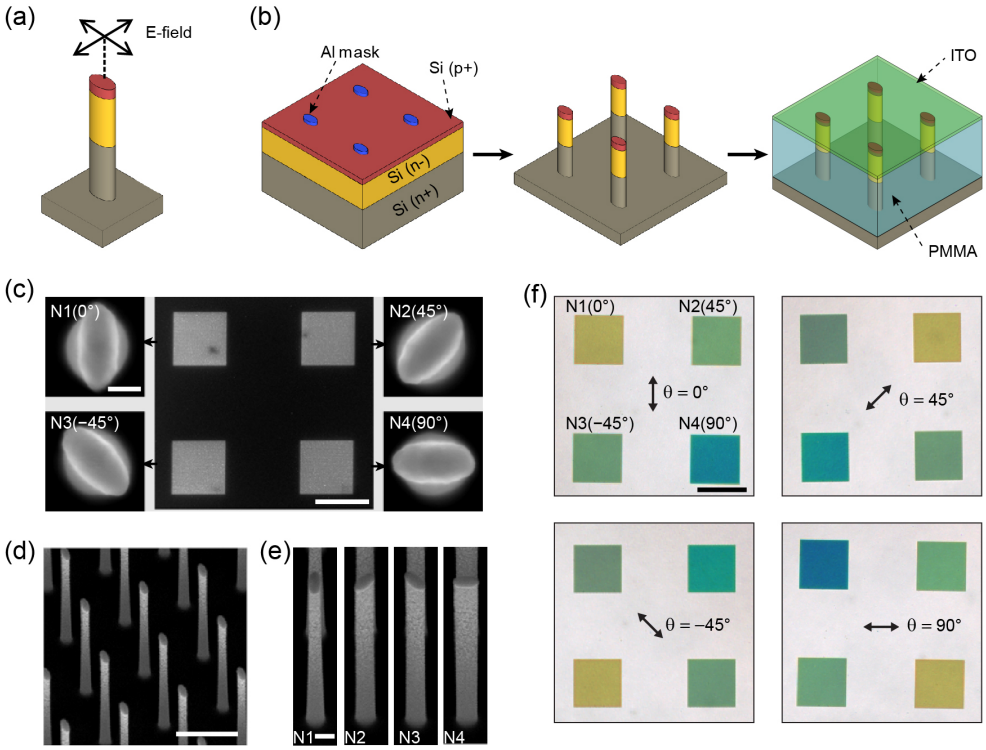

Fig. 1. Elliptical silicon nanowire photodetectors. (a) Schematic concept of our device. Nanowire's absorption depends on polarization of incident light. (b) Fabrication process for elliptical silicon nanowire photodetectors. An epitaxial wafer with p+/n-/n + layers is prepared. Etch mask that comprises aluminum elliptical disks is patterned on wafer and dry etching is performed to fabricate vertical nanowires. PMMA spacer is fabricated and transparent top contact (ITO) is deposited. (c) SEM image of elliptical nanowires after dry etching. Four elliptical nanowire arrays with four different orientations are fabricated (image in center). Scale bar is 100 µm. Magnified views (side images) of arrays (N1, N2, N3 and N4) show that constituent nanowires have orientations of 0°, 45°, –45° and 90°. Scale bar in magnified image is 100 nm. (d) Tilted (30°) SEM view of elliptical nanowire array. Scale bar is 1 µm. (e) Side view of nanowires from four arrays. Scale bar is 200 nm. (f) Optical microscope images of elliptical nanowire arrays under linearly polarized illumination. Arrow indicates polarization of incident light (polarization angle θ = 0°, 45°, –45° and 90°). Scale bar is 100 µm.

We fabricate four arrays of elliptical nanowires. The arrays differ by the orientation of the constituent nanowires. These allow calculation of the first three Stokes parameters. These allow determination of angle of polarization (AOP) and degree-of-linear polarization (DOLP) [5]. The nanowire arrays are denoted N1(0°), N2(45°), N3(–45°) and N4(90°). The angle in parenthesis refers to the orientation of the elliptical nanowires of the array. Figure 1(c)–1(e) are scanning electron microscope (SEM) images of our device. The heights of fabricated nanowires are 2.7 µm. The nanowires are formed in square arrays with pitch 1 µm. Each array has 10,000 elliptical nanowires. Each array has an extent of 100 µm × 100 µm. The elliptical nanowire have radii of 60 nm and 120 nm along their short and long axes, respectively. These radii are the design values in the electron beam lithography step. Each nanowire has an axial p-i-n junction. The thicknesses of each p+/n-/n + layers are 200 nm / 1200 nm / 1300 nm. Figure 1(f) shows that the color of each array depends on the angle between the polarization axis of the illuminating light and the orientation of the elliptical nanowires.

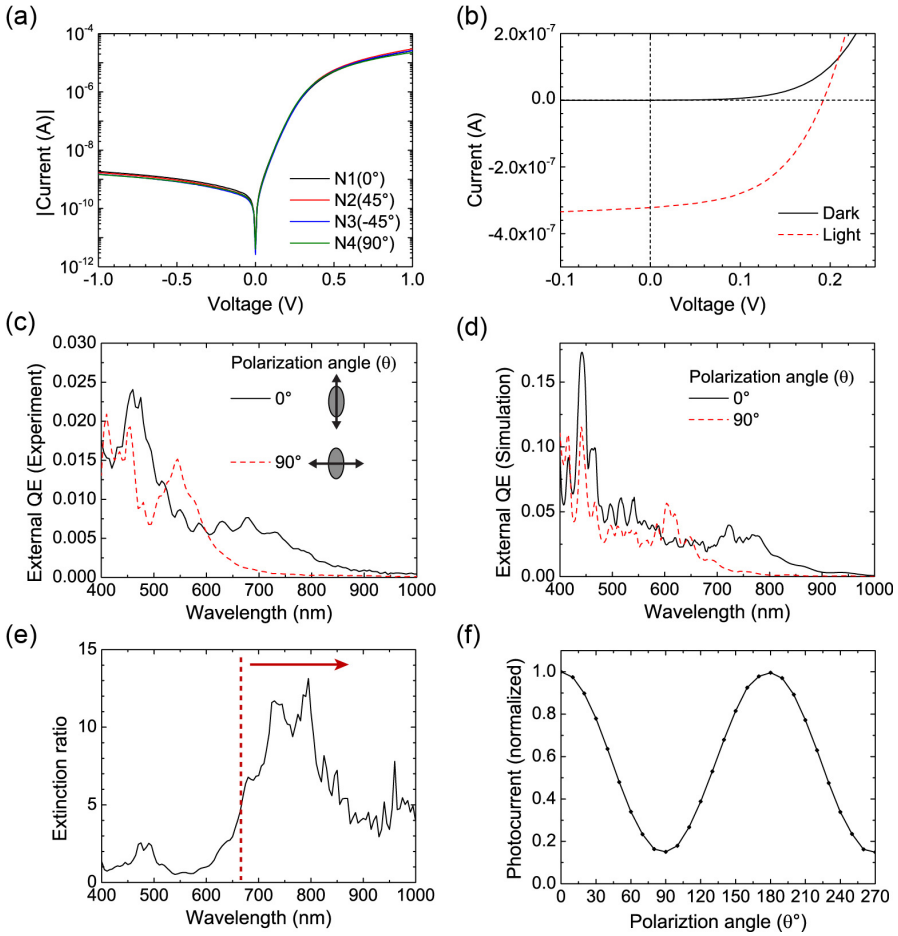

Fig. 2. Measurements of fabricated devices. (a) Log scale I-V curve of nanowire arrays in dark (no illumination). (b) I-V curve of array N4(90°) in dark / under illumination of 820 mW / cm^2 at a wavelength of 633 nm. Light is linearly polarized parallel to long axis of elliptical nanowires (θ = 90°). (c) Measured external quantum efficiencies (QE) spectra of array N1(0°) under vertically- and horizontally-polarized illumination (θ = 0°, θ = 90°). (d) Simulated external QE spectra of array N1(0°). (e) Extinction ratio calculated from measured external QE of Fig. 2(c). Dotted line indicates cut-off wavelength ($\lambda_{cut\text{-}off}$ = 665 nm) of long pass filter used in later experiments. (f) Normalized photocurrent at wavelength of 700 nm as a function of polarization angle θ.

We measure current-voltage (I-V) characteristics for fabricated nanowire arrays [Fig. 2(a)]. These measurements are conducted in a dark environment at room temperature. A general purpose sourcemeter (2400, Keithley) is used for the current-voltage curve measurements. We sweep the voltage from −1 V to 1 V in 0.01 V steps and measure the current. The dark current is ~2 nA at a bias of −1V. Figure 2(b) shows measured I-V characteristics of the N4(90°) array under dark and illuminated conditions. We next measure the responsivities of our device under the linearly-polarized light. Light from a monochromator (MS257, Oriel instruments, λ = 400–1000 nm, 10 nm step) goes into a pinhole (diameter: 200 μm), then passes through a polarizer (10GT04, Newport). The resultant linearly polarized light is focused onto the nanowire array using an objective lens (magnification 10 × , NA 0.28, Mitutoyo). A 50:50 non-polarizing cube beam splitter is installed between the pinhole and polarizer in order for the light reflected from the nanowire device to be collected and imaged onto a charge-coupled device camera (DMK21AU04, Imaging Source). A picoammeter (6485, Keithley) measures photocurrent from the N1(0°)

array in photovoltaic mode (0V bias). Using measured responsivities of the nanowire devices, their external quantum efficiencies are calculated. It is clearly seen that the elliptical nanowires have polarization dependent spectral response [Fig. 2(c)]. Finite-difference time-domain (FDTD) simulations are performed and the results are shown in Fig. 2(d). We assume an internal quantum efficiency (QE) of 100%. The simulation results for elliptical nanowires with radii of 40 nm / 80 nm along short / long axis are in reasonable agreement with measured external QE lineshapes. This dimensional discrepancy between the response of the actual device and the predictions of simulations could be due to imperfect fabrication. We estimate that internal QE of our device is 20% from the comparison of measurements and simulations. Our nanowire photodetectors have lower internal QE than conventional silicon photodetectors because of surface recombination that originates from the larger surface-to-volume ratio and surface damage resulting from the dry etching process [33].

From the measured QE spectra [Fig. 2(c)], we find the extinction ratio as the QE for light polarized along the nanowire's long axis divided by the QE for light polarized along the short axis. The results are shown in Fig. 2(e). Because the absorption of nanowire array depends on wavelength and has a multiple peak nature [28, 34, 35], the extinction ratio varies with the wavelength. It can be seen that the external QE of the array N1(0°) under vertically polarized illumination (0°) is higher than that under horizontally polarized illumination (90°) in the wavelength range from 600 nm to 1000 nm. We therefore put a long pass filter with a cut-off wavelength of 665 nm in front of the nanowire device to perform polarization-resolved imaging. For $\lambda > 665$ nm, the elliptical nanowire photodetector has an extinction ratio exceeding 2.9. Figure 2(f) shows the normalized photocurrent of array N1(0°) as a function of polarization angle (θ), illumination at $\lambda = 700$ nm. It can be seen that the response approximately follows Malus's law, being approximately proportional to $\cos^2\theta$.

Polarization-resolved imaging is performed using the elliptical nanowire photodetectors. Images of 3-D glasses [Fig. 3(a)] that have pairs of orthogonal linear polarizer (orientation: 45° and −45°) are taken. A single-lens reflex (SLR) camera lens (focal length: 50 mm) operated at an f / 2.0 is used for imaging experiments. A long pass filter with cut-off wavelength of 665 nm (FGL665S, Thorlabs) is installed between the camera lens and the nanowire device. Two incandescent bulbs (60 W each) illuminate the front side of the 3-D glasses and one incandescent bulb (60 W) illuminates the back side of the 3-D glasses. Two motorized linear stages (T-LSM050A, Zaber Technologies) are used for mechanical scanning of our nanowire device. We measure photocurrents from the four arrays (N1, N2, N3 and N4) in an array of 150 × 150 positions with a scanning step of 119 μm. It can be clearly seen that each polarization filter of the 3-D glasses has a brightness that varies with the angle between its polarization axis and the orientation of the elliptical nanowires of the array. We next calculate the degree-of-linear polarization (DOLP) and the angle of polarization (AOP) [5]. The polarization filters of the 3-D glasses are measured to exhibit high DOLP values as expected [Fig. 3(b)]. The DOLP values measured by our nanowire devices [Fig. 3(b)] are lower than their true values however, due to the limited extinction ratio of our devices [36]. From Fig. 3(c), it can be seen that the AOP images produced by our nanowire devices correctly display the orientations of the polarization axes of polarizers in the 3-D glasses.

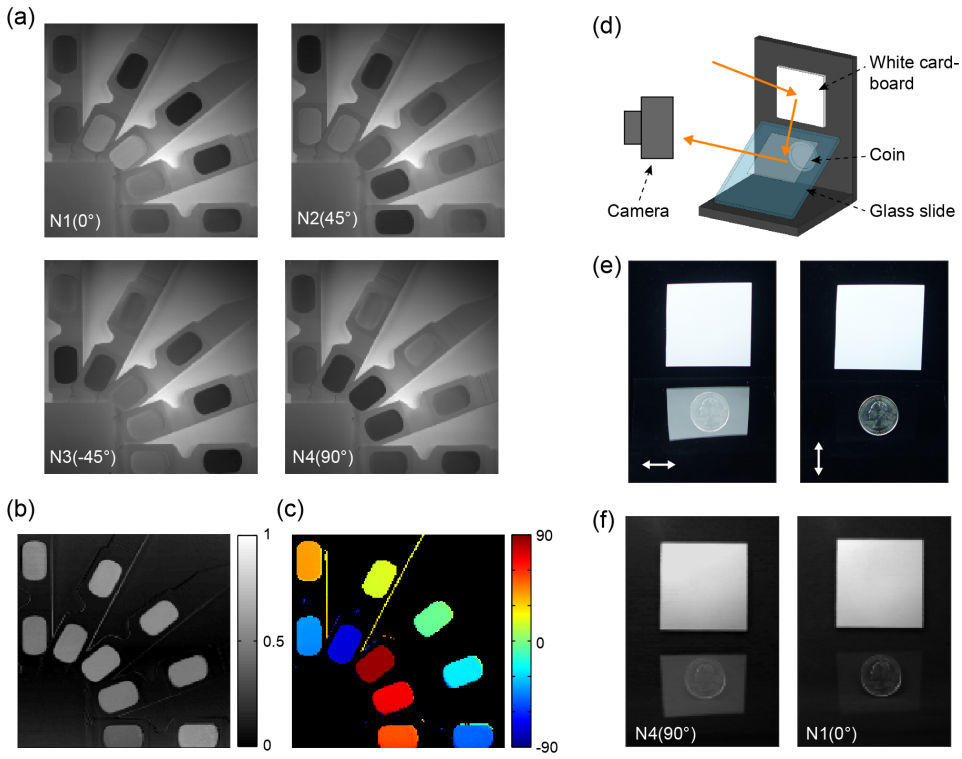

Fig. 3. Polarization-resolved imaging using fabricated device. (a) Images captured by nanowire arrays N1(0°), N2(45°), N3(–45°) and N4(90°) (b) Degree-of-linear polarization (DOLP) image found from images of Fig. 3(a). (c) Angle of polarization (AOP) image found from images of Fig. 3(a). (d) Schematic of experimental setup used for demonstrating polarization-resolved imaging with nanowire device. Coin below glass slide cannot be seen clearly due to strong reflection from glass. (e) Image taken by conventional camera with horizontal and vertical polarization filters. Arrow indicates axis of polarization filter. (f) Images captured by our elliptical nanowire arrays N4(90°) and N1(0°). Gamma correction of 1 / 2.2 is applied.

The most ubiquitous approach in which polarization is used to improve imaging contrast is that of polarized sunglasses. Glare from horizontal surfaces, e.g. water, is polarized parallel to these surfaces. In order to reduce this glare, polarized sunglasses therefore comprise filters that transmit vertical polarization. We next demonstrate that our elliptical nanowire photodetectors can achieve this functionality. Figure 3(d) shows the experimental setup. A tilted glass slide is situated near a piece of white cardboard attached to a vertical surface. Light can be reflected or scattered by the white cardboard and then reflected by the glass slide. This reflected light reduces the visibility of the object (coin) under the glass slide. Figure 3(e) shows images taken by a conventional camera with horizontal and vertical polarization filters. Two incandescent bulbs (60W each) are used for front side illumination. When the horizontal polarization filter is used, the resultant image shows a strong reflection from the glass slide. By contrast, this reflected light is suppressed and the coin is clearly seen when the vertical polarization filter is used. We take images of the same scene using our elliptical nanowire photodetectors [Fig. 3(f)]. In the image recorded by array N1(0°), the reflection from the glass slide is suppressed, and the visibility of the coin is enhanced.

3. Conclusion

In summary, we have developed polarization-resolving photodetectors comprising vertical silicon nanowires with elliptical cross-sections. This approach is very different from that employed in division-of-focal plane imaging polarimeters based on polarization filter arrays.

In such devices, the unwanted polarization is discarded via absorption (or reflection) by the filter. By contrast, in our approach, absorbed light is converted to photocurrent. In our current configuration, the light not absorbed by the elliptical nanowires is largely transmitted into the substrate. This light can be converted to photocurrent by incorporating an additional photodetector in the substrate. This will allow us the compelling possibility of polarization-resolving pixels with high efficiency.

Acknowledgments

This work was supported in part by the National Science Foundation (NSF, grant no. ECCS-1307561), by the Australian Research Council's Discovery Projects funding scheme (project number DP150103736) and by the Victorian Endowment for Science, Knowledge and Innovation (VESKI). Fabrication work was performed at the Center for Nanoscale Systems (CNS) at Harvard, which is supported by the NSF.